Materials International
Open-Access Journal (ISSN: 2668-5728)

*Article*
**Volume 8, Issue 1, 2026, 3**
https://doi.org/10.33263/Materials81.003

# Green Nanoparticles from *Alpinia officinarum* Suppress Growth and Biofilm Formation in Gram-Positive Bacteria

**Narmadha Alagirisamy [1], Hemalatha Srinivasan [1,*]**

[1] School of Life Sciences, B. S. Abdur Rahman Crescent Institute of Science & Technology, Chennai, India
* Correspondence: hemalatha.sls@bsauniv.ac.in;

**Received: 6.10.2025; Accepted: 15.01.2026; Published: 10.03.2026**

**Abstract:** Nanotechnology is a well-established field of science. The green synthesis of nanoparticles is cost-effective and safe. In this study, silver nanoparticles (AgNPs) were synthesized from Alpinia officinarum rhizome extracts, which were polymorphic, polydispersed, and of a wider size, as confirmed by physicochemical characterization. AgNPs' antimicrobial activity was screened against human, poultry, and cow mastitis Staphylococcus sp. The AgNPs displayed strong antibacterial activity, with inhibition rates of 23.08% for MRSA, 19.66% for MTCC strains, 30.17% for MDR isolates, 26.17% for *S. arlettae*, 42.55% for *S. cohnii*, and 32.85% for both *S. sciuri* and *S. chromogenes*. The highest MBC was recorded at 50 µg/mL, while the lowest was at 25 µg/mL. Furthermore, the nanoparticles effectively inhibited biofilm formation, with *S. sciuri* showing the highest inhibition (19.14%), as verified by biochemical assays. AgNPs treatment induced sugar and protein leakage and oxidative stress, which led to the release of malondialdehyde and reduced SOD, GSH, and CAT enzyme activities. The results revealed that AgNPs were effective in controlling growth and biofilm formation by inducing oxidative stress, interfering with antioxidant enzymes, and inducing cell content leakage in the Staphylococcus sp. This study demonstrates that AgNPs are a sustainable and effective alternative for treating Staphylococcus infections and biofilm-related complications.

**Keywords:** *Alpinia officinarum*; *Staphylococcus aureus*; antibacterial activity; green synthesis; silver nanoparticles; antibiofilm.



## 1. Introduction

Nanotechnology, an emerging interdisciplinary field, has transformed diverse scientific areas, including medicine, diagnostics, and materials engineering. Among nanomaterials, silver nanoparticles (AgNPs) have gained particular attention due to their strong antimicrobial, antioxidant, and catalytic properties. Conventional physical and chemical methods for synthesizing nanoparticles often involve toxic reagents, high energy consumption, and hazardous by-products. In contrast, green synthesis using biological sources offers a safer, eco-friendly, and cost-effective alternative, utilizing natural reducing and stabilizing agents from plants, bacteria, or fungi [1-3].

Plant-mediated synthesis of AgNPs has become increasingly significant, as phytochemicals such as flavonoids, terpenoids, phenolics, and alkaloids serve dual roles in reducing silver ions and capping the resulting nanoparticles, enhancing their stability and bioactivity. Recent studies have reported that green-synthesized AgNPs exhibit potent

antibacterial and antibiofilm effects against multidrug-resistant (MDR) pathogens, including Staphylococcus aureus. However, limited attention has been given to their effects on coagulase-negative Staphylococcus (CoNS) species—such as S. arlettae, S. cohnii, S. sciuri, and S. chromogenes—which are emerging opportunistic pathogens in both human and veterinary infections. These species, commonly associated with mastitis and device-related infections, can form robust biofilms and serve as reservoirs for antibiotic resistance genes, complicating treatment outcomes [4-6].

Alpinia officinarum (lesser galangal), a medicinal rhizomatous plant of the Zingiberaceae family, is rich in bioactive phytochemicals, including flavonoids (galangin, kaempferide), phenolics, and essential oils such as 1,8-cineole and eugenol. These compounds possess strong reducing and antioxidant properties, making the plant a suitable candidate for green nanoparticle synthesis. Although previous studies have highlighted the medicinal potential of *A. officinarum*, its role in the biogenic synthesis of AgNPs and their antibacterial mechanisms against MDR and CoNS Staphylococcus species remains underexplored [7].

Therefore, the present study aimed to: Synthesize and characterize silver nanoparticles using *A. officinarum* rhizome extracts through physicochemical and microscopic techniques; Evaluate their antibacterial and antibiofilm activities against Staphylococcus aureus (MRSA (ATCC 33591), MTCC (MTCC 6908), and MDR isolates) and coagulase-negative *Staphylococcus* species (*S. arlettae*, *S. cohnii*, *S. sciuri*, *S. chromogenes*); and Elucidate the underlying mechanisms of action of the biosynthesized AgNPs by assessing oxidative stress induction, leakage of cellular contents, and alterations in antioxidant enzyme activities.

This study provides insights into the potential of *A. officinarum*-derived AgNPs as a sustainable and effective strategy for combating drug-resistant *Staphylococcus* infections and biofilm-associated complications.

## 2. Materials and Methods

### *2.1. Preparation of rhizome extracts from Alpinia officinarum.*

Fresh rhizomes of *Alpinia officinarum* were washed thoroughly with distilled water, shade-dried, and ground into a fine powder using a mechanical grinder. A total of 10 g of rhizome powder was mixed with 100 mL of double-distilled water (final concentration: 10 % w/v) in a 250 mL Erlenmeyer flask. The mixture was maintained at 37°C on a rotary shaker at 150 rpm for 12 h to facilitate the extraction of bioactive compounds. After incubation, the mixture was cooled to room temperature (approximately 25°C) and allowed to settle for 30 min. The supernatant was then filtered through Whatman No. 1 filter paper, followed by a second filtration through a 0.45 µm membrane filter to remove residual particles. The pH of the extract was measured (approximately pH 6.8 ± 0.2), and no adjustment was made. The resulting aqueous extract was stored at 4°C in an amber glass bottle until further use for nanoparticle synthesis [8].

### *2.2. Synthesis of AgNPs.*

AgNPs were synthesized by mixing 500 mL of *A. officinarum* rhizome extract with 1000 mL of 1 mM $AgNO_3$ solution (1:2 ratio) under continuous stirring. The reaction mixture was exposed to light irradiation for 1 hour until a characteristic brown coloration appeared, indicating nanoparticle formation, which was confirmed using UV–Vis spectroscopy. The

suspension was centrifuged at 13,000 × g for 15 min at 4°C, and the resulting pellet was washed three times with double-distilled water to remove unbound phytochemicals and residual ions, with each wash followed by centrifugation under the same conditions. The final pellet was re-dispersed in 30% DMSO (v/v) stock solution, and the suspension was sonicated on ice for 10 min to ensure uniform nanoparticle dispersion. For biological assays, this stock was diluted to a working concentration containing ≤1% DMSO, which does not affect bacterial cell viability.

*2.3. Physicochemical characterization of AgNPs.*

The synthesized silver nanoparticles (AgNPs) were characterized using multiple physicochemical techniques to confirm their formation, morphology, and structural properties.

2.3.1. UV–visible spectrophotometer.

The UV–Visible spectrophotometer (Shimadzu UV-2600, Japan) was used to monitor the synthesis of AgNPs by recording absorbance spectra over 300–700 nm, confirming the surface plasmon resonance (SPR) characteristic of silver nanoparticles.

2.3.2. Fourier transform infrared spectroscopy.

Fourier Transform Infrared Spectroscopy (FTIR; Bruker Alpha II, Germany) was performed in the range of 400–4000 $cm^{-1}$ to identify the functional groups of phytochemicals responsible for the reduction and stabilization of $Ag^{+}$ ions during nanoparticle synthesis.

2.3.3. The field emission scanning electron microscopy.

The Field Emission Scanning Electron Microscopy (FESEM; JEOL JSM-7610F) was used to determine the surface morphology and approximate particle size of AgNPs, while Energy Dispersive X-ray (EDX) analysis confirmed the elemental composition and presence of silver in the reaction mixture.

2.3.4. X-ray diffraction.

X-ray Diffraction (XRD; PANalytical X'Pert PRO) was conducted using Cu Kα radiation (λ = 1.5406 Å) over a 2θ range of 20°–80° to determine the crystalline nature of the AgNPs.

2.3.5. Dynamic light scattering.

Dynamic Light Scattering (DLS; Malvern Zetasizer Nano ZS) was employed to measure the hydrodynamic diameter and zeta potential, providing information on particle size distribution and surface charge stability.

2.3.6. High-resolution transmission electron microscopy.

The detailed morphology and lattice structure of the nanoparticles were examined using High-Resolution Transmission Electron Microscopy (HRTEM; JEOL JEM-2100), and selected area electron diffraction (SAED) patterns were analyzed to confirm the crystalline structure.

2.3.7. X-ray photoelectron spectroscopy.

Finally, X-ray Photoelectron Spectroscopy (XPS; Thermo Scientific K-Alpha) was used to determine the elemental composition, oxidation state, and binding energy of silver and associated elements in the AgNPs.

*2.4. Assays to explore antimicrobial and antibiofilm activity of AgNPs.*

The antibacterial activity of the biosynthesized AgNPs was evaluated by determining the Minimum Inhibitory Concentration (MIC) and Minimum Bactericidal Concentration (MBC) using the broth microdilution method following CLSI guidelines (2023).

AgNPs were assessed for antibacterial activity by measuring MIC, MBC, and biofilm assay using MRSA, MTCC, MDR species of *S. aureus*, *Staphylococcus arlettae*, *Staphylococcus cohnii*, *Staphylococcus sciuri*, and *Staphylococcus chromogenes* incubated overnight in LB broth. The inoculum density used for the MIC and MBC assays was standardized to $1 \times 10^6$ CFU/mL, which was adjusted by comparing the bacterial suspension turbidity to a 0.5 McFarland standard prior to use.

MIC was performed in triplicate, 100 µL of LB broth was added to a 96-well plate, and 100 µL of nanoparticles were added to the first well and were serially diluted, 2 µL of bacterial culture was added to each well, and the plate was kept in a shaker incubator for 24 hours at 100 rpm at 37°C. OD was taken at 600 nm in a multimode plate reader, and MIC was calculated. MBC was performed to determine the minimum level of AgNPs required to kill the microorganism. 24-hour plates were used, 2 µL of bacterial culture was plated and incubated in a shaker incubator, and the concentration at which the organisms were totally killed is marked as MBC.

In biofilm assay plate was incubated for 48 hours and were completely dried and 150 microliters of 0.1 % crystal violet was added, incubated for 20 mins and washed twice and 30 % glacial acetic acid was added and kept for 15 mins, reading was taken after 15 mins using multimode plate reader at 580 nm (Perkin Elmer Inspire multimode reader) which revealed antibiofilm activity of silver nanoparticles. All the experiments were performed in triplicate.

*2.5. Biochemical assays.*

2.5.1. Reduction of total sugars and proteins.

Anthrone and Bradford were used for the estimation of reduction of total sugars and proteins, The effect of AgNPs on protein and sugar leakage was assessed by treating *Staphylococcus sp* with AgNPs at their MIC which was incubated for 12 hrs, after incubation samples were centrifuged at 10,000 rpm for 30 mins at 4°C, the resultant supernatant were stored in 4°C for further estimation of protein and sugar.

2.5.2. Estimation of glutathione reductase.

AgNPs-treated and untreated *Staphylococcus* sp. were centrifuged at 10,000 rpm for 5 mins, then washed with PBS, and simultaneously, the cells were lysed with phenol, chloroform, and then to the aqueous extract, DTNB was added, and the absorbance was measured at 412 nm.

2.5.3. Estimation of malondialdehyde.

*Staphylococcus* sp. in LB broth was assessed for malondialdehyde using thiobarbituric acid. 10 % SDS was treated with 1 ml of AgNPs-treated cells and vigorously whirled and incubated for 60 mins at 95°C with 2 ml thiobarbituric acid, and it was centrifuged at 5000 rpm for 10 mins after cooling to room temperature, and the absorbance was measured at 530 nm.

2.5.4. Estimation of catalase and superoxide dismutase.

AgNPs-treated and untreated cells were pelleted down and washed with PBS. To the pellet addition of 50 mM PBS with PH 7.0, 15 mM hydrogen peroxide was added, and the reduction of $H_2O_2$ was measured at 240 nm absorbance. To the 100 µL of silver nanoparticles treated and untreated pellet, 20 µL of 50 mM PBS, 20 µL of 13 mM methionine, 20 µL of 63 mM nitroblue tetrazolium, and 20 µL of 1.3 mM riboflavin were added. This mixture was incubated in the dark for 15 minutes, and the OD value was measured at 560 nm to estimate the superoxide dismutase.

*2.6. Statistical analysis.*

Experimental assays were conducted in triplicate (n = 3) to confirm the reproducibility and reliability of results. The data from experiments were collected and analyzed statistically. Microsoft Excel (MS Excel) was utilized for plotting the graphs and carrying out statistical calculations, such as mean value determination, standard deviations (SD), and Student's t-test.

## 3. Results and Discussion

*3.1. Synthesis and characterization of AgNPs.*

AgNPs synthesized from *A. officinarium* rhizome extracts by adding silver nitrate in a 1:2 ratio showed colour change, which indicated the reduction of silver ions into AgNPs, and the synthesis is confirmed by UV-vis spectroscopy, as shown in Figure 1a. It is a common, dependable method for the primary characterization of nanoparticles. AgNPs have specific optical properties so that they highly interact with specific wavelengths of light [9, 10]. Here in this study, AgNPs were characterized by UV-VIS spectroscopy, which confirmed the presence of AgNPs with a surface plasmon resonance peak observed at 400 nm, while the peak of *Alpinia officinarum* rhizome extracts was observed at 500 nm, as shown in Figure 1a. AgNPs were further characterized by using FT-IR showed functional groups present in both AgNPs and rhizome extracts as shown in figure 1b and 1c, The extracellular synthesis of the AgNPs from rhizome extract of *Alpinia officinarum* revealed absorption spectrum in the range of 400 to 3600 $cm^{-1}$, FTIR is highly used to check the involvement of biomolecules in the synthesis of nanoparticles, footprints of functional group are alkyne, alkene, terminal alkyne, aryl, alkyne, aryl disulphide etc [Table 1]. It confirms that phytocompounds are utilized for AgNPs synthesis [11].

XRD pattern of AgNPs synthesized from *Alpinia officinarum* shows distinct peaks at specific 2θ values, confirming that the synthesized AgNPs are crystalline. In this study, the XRD peaks at various 2θ positions are consistent with the FCC structure of silver, indicating that the nanoparticles are well-crystallized and not amorphous. The 2θ values corresponding to

the (111), (200), (220), and (311) planes are characteristic reflections for crystalline AgNPs with an FCC structure, as shown in Figure 1d.

**Table 1.** FT-IR analysis and the functional group of AgNPs and *Alpinia officinarum* rhizome extracts.

| Wave number (cm-1) of AgNPs | Functional group of AgNPs | Compound class | Wave number (cm-1) rhizome extracts | Functionality of the group of rhizome extracts | Compound class |
|---|---|---|---|---|---|
| 3642 | Nonbonded hydroxy group, OH stretch | alkyne | 3297 | O-H Stretching | Carboxylic acid |
| 2905 | Methyl (−$CH_3$) | Saturated Aliphatic (alkene/alkyl) | 2924 | C-H stretching | Methyl group |
| 2143 | C≡C Terminal alkyne (monosubstituted) | C≡C alkene | 2199 | C≡C Stretching | aromatic alkene |
| 1639 | C=C stretching | Aromatic ring (aryl) | 1637 | C=C stretching | Quinone or conjugated ketone |
| 1001 | C-F stretching | Phosphate ion | 1010 | Cyclohexane ring | Methylene |

The (111) plane typically shows the highest intensity in XRD patterns for FCC metals like silver, indicating that this is the most dominant and stable crystal orientation. (200), (220), and (311) Planes: These planes reflect the typical arrangement of atoms in the FCC lattice and confirm the multi-faceted crystalline structure of AgNP. Matching the XRD peaks with the JCPDS file no. 04-0783 confirms that the synthesized material is indeed elemental silver in its standard crystalline FCC structure. This comparison also rules out impurities or undesired phases that might have formed during synthesis [12,13].

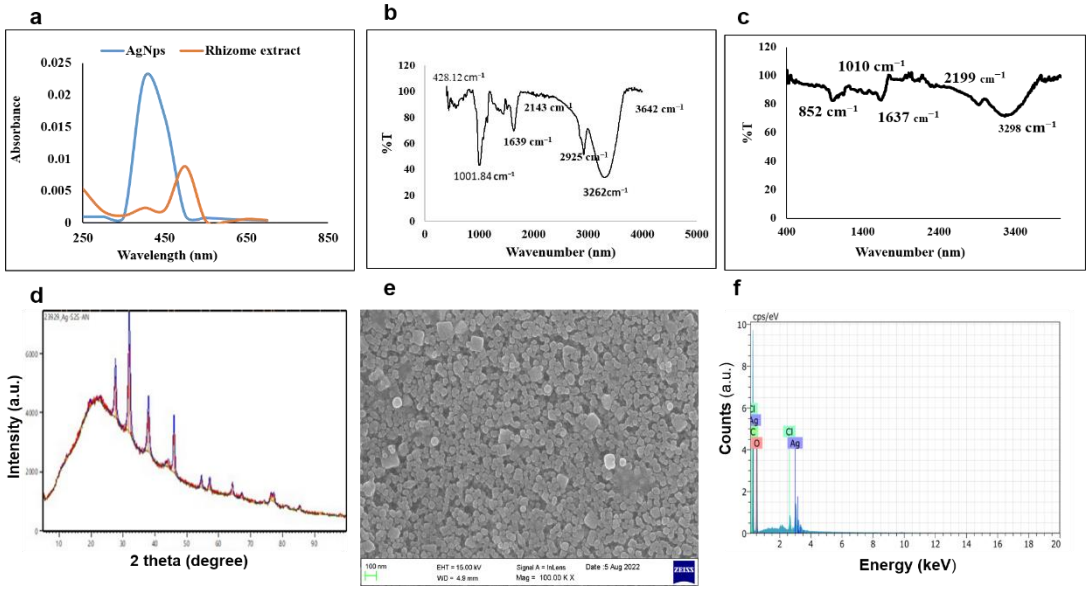


**Figure 1.** Characterization of silver nanoparticles (AgNPs) synthesized from the rhizome extracts of *Alpinia officinarum*. **(a)** UV–Visible absorption spectra of the synthesized AgNPs and the *A.officinarum* rhizome extract; **(b)** FTIR spectrum of the synthesized AgNPs; **(c)** FTIR spectrum of the *A. officinarum* rhizome extract; **(d)** XRD diffraction pattern confirming the crystalline nature of the AgNPs; **(e)** FESEM micrograph of the AgNPs at 100× magnification showing surface morphology; **(f)** EDX spectrum confirming the elemental composition of the synthesized AgNPs.

FESEM is a surface-imaging method that probes particle morphology. The combination of FESEM and EDAX examines silver powder morphology and analyzes its chemical composition. Here in this study, FESEM reveals the morphology and size of AgNPs. The shape

of the particle is polymorphic and polydispersed, and the width is 4.9 mm at 100KX magnification, as shown in Figure 1e. The polymorphic nanoparticles were due to the presence of phytocompounds in rhizome extracts of *Alpinia officinarum* [14, 15].

EDAX (Energy Dispersive X-ray Analysis) is a useful tool to confirm the elemental composition of AgNPs synthesized from the rhizome of *Alpinia officinarum*. EDAX confirms the presence of silver and detects other elements present from the plant rhizome extract that might be adhered to the nanoparticle surface. EDAX spectrum shows the presence of Ag, Cl, $O_2$, carbon, and an AgNPs peak is detected at 5.5 keV. The presence of oxygen reveals the formation of organic residues from the plant, which could coat or stabilize the AgNPs. Carbon peaks usually arise from phytochemicals in the plant extract that may adhere to the nanoparticle surface, thereby capping and stabilizing the nanoparticles. The presence of plant-derived elements in the spectra confirms that *Alpinia officinarum* components likely stabilize and cap the AgNPs, thereby enhancing their stability and biocompatibility. EDAX spectroscopy assesses the primary composition of AgNPs as shown in Figure 1f.

DLS result shows the size and distribution of the AgNPs. The Polydispersity Index (PDI) is a measure of particle size distribution in the solution. A lower PDI suggests a high constant particle size, while an advanced polydispersity index specifies a wider size distribution. The particle size of AgNPs was 609.2 nm, and the polydispersity index value was 0.728 nm and displayed an intercept at 0.868 as revealed in Figure 2a. DLS provides the hydrodynamic diameter of AgNPs, which includes not just the metal core but also the surrounding organic shell or capping agents from the *Alpinia officinarum* rhizome extract. The size of the AgNPs varies with the concentration of Alpinia officinarum rhizome extracts used during synthesis, as this influences the formation of the nanoparticle core and the thickness of the organic capping layer. DLS results typically show a higher particle size than that observed in TEM (Transmission Electron Microscopy) due to the plant extract's hydration layer and organic coating [16]. The dynamic light scattering (DLS) analysis showed an average hydrodynamic diameter of 609 nm, which is substantially larger than the particle sizes observed in FESEM and HRTEM analyses. This apparent discrepancy can be attributed to the fundamental differences in the measurement principles of these techniques. DLS measures the hydrodynamic diameter, which includes not only the metallic core of the nanoparticles but also the capping layer of phytochemicals, solvation shell, and any weakly associated nanoparticle aggregates in the colloidal suspension. In contrast, FESEM and HRTEM provide direct imaging of the metallic core, typically under dry or vacuum conditions, without contributions from solvent or capping molecules.

The zeta potential, zeta deviation, and conductivity values for AgNPs synthesized using *Alpinia officinarum* rhizome extracts offer major insights into the AgNPs' stability and surface characteristics. The zeta deviation shows variability in the zeta potential measurements and gives insight into the homogeneity of the particle surface charge. The zeta potential value of AgNPs was 5.30 mV, zeta deviation 5.98 mV, and the conductivity was 0.0155 (mS/cm). A zeta deviation of 5.98 mV is relatively high, implying a broad range in surface charges across different particles in the sample. This variation could result from inconsistent capping or uneven distribution of the organic molecules from the *Alpinia officinarum* extract on the nanoparticle surface. Zeta potential reveals positive charge and polymorphic nature of the AgNPs as shown in Figure 2b. Zeta potential is a major factor in assessing a nanoparticle’s surface charge. It is used to calculate the dispersion's stability in a colloidal solution, which

refers to the ability of the nanoparticles and any ions present to conduct an electric current. A conductivity of 0.0155 mS/cm is low, suggesting that there are minimal free ions in the solution, possibly due to the stability imparted by the plant extract. Low conductivity implies that the nanoparticles are dispersed in a medium with low ionic strength, which might help prevent aggregation in systems with low zeta potential, as there are fewer ions to screen the weak surface charge on the nanoparticles [17].

HR-TEM reveals polydispersity, indicating heterogeneous size distribution. Polydispersity typically suggests that the synthesis method produces particles of varying sizes rather than a uniform size, as shown in Figure 2c. In AgNPs, size influences surface plasmon resonance (SPR). Polydisperse distribution can broaden the SPR peak in UV-Vis spectroscopy, as particles of different sizes resonate at slightly different frequencies. Polydispersed nanoparticles may have different aggregation tendencies. Smaller particles with higher surface energy aggregate faster than larger particles, leading to uneven distribution in applications or reduced effectiveness in colloidal suspensions. Polydispersed AgNPs can exhibit unique characteristics with varying size distributions, whereas size uniformity affects properties such as stability, catalytic efficiency, and optical behavior [18, 19].

The SAED pattern of AgNPs typically shows concentric rings, and the particles are randomly oriented. These rings are formed due to constructive interference from the crystal planes aligned in various orientations, as shown in Figure 2d. The spacing between the rings is used to identify the crystal structure, which can be matched to the known lattice parameters of silver.

SAED of AgNPs provides a fingerprint of their crystalline structure and reveals essential information about the nanoparticle's phase, crystallinity, size distribution, and presence of any structural defects. This information is crucial for understanding and optimizing the material for various applications [20-22].

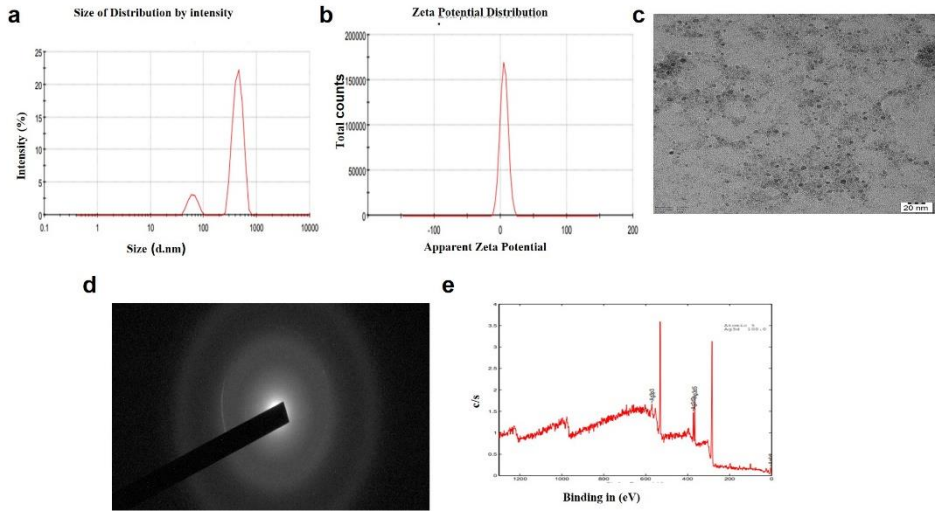


**Figure 2.** Characterization of silver nanoparticles (AgNPs) synthesized from the rhizome extract of *Alpinia officinarum*. **(a)** Dynamic light scattering (DLS) analysis showing the particle size distribution of the synthesized AgNPs; **(b)** Zeta potential measurement indicating the surface charge and colloidal stability of the AgNPs; **(c)** High-resolution transmission electron microscopy (HR-TEM) image depicting the morphology and nanoscale size of the AgNPs; **(d)** Selected area electron diffraction (SAED) pattern confirming the crystalline structure of the AgNPs; **(e)** X-ray photoelectron spectroscopy (XPS) spectrum demonstrating the elemental composition and chemical states present on the surface of the synthesized AgNPs.

XPS confirms the presence of silver by detecting characteristic peaks corresponding to silver's core-level electrons. XPS reveals the atomic state of the silver nanoparticle and

elemental and binding energy in 380 keV as Ag3d5, Ag3p3. XPS confirms the presence of silver in the atomic state Agd5 and Agp3; these peaks are a strong indicator of elemental silver (Ag) and confirm the composition of the nanoparticles, as shown in Figure 2e. XPS helps verify the presence of functional groups from capping agents, which are important for preventing aggregation, enhancing biocompatibility, or improving dispersion in various solvents. Together, SAED and XPS provide complementary confirmation of the AgNPs' crystalline structure, elemental composition, and surface chemistry, essential for their functional performance [23-27].

*3.2. Antimicrobial and antibiofilm activity of AgNPs.*

Minimal inhibitory concentration is the lowest level at which AgNPs inhibit the microbe's growth [25]. The AgNPs treatment reduced MRSA growth to 23.08%, MTCC 19.66%, and 30.17% in MDR clinical isolates of *S. aureus*. The highest MBC of AgNPs was found at 50µg/ml, and the minimum was found at 25 µg/ml after 12 hours of treatment (Figure 3a). MIC in which the growth of poultry species after nanoparticle treatment was *Staphylococcus arlettae* 26.17 %, *Staphylococcus cohnii* 42.55 %, *Staphylococcus sciuri* 32.85 %, and *Staphylococcus chromogenes* 32.85 % as shown in Figure 3a.

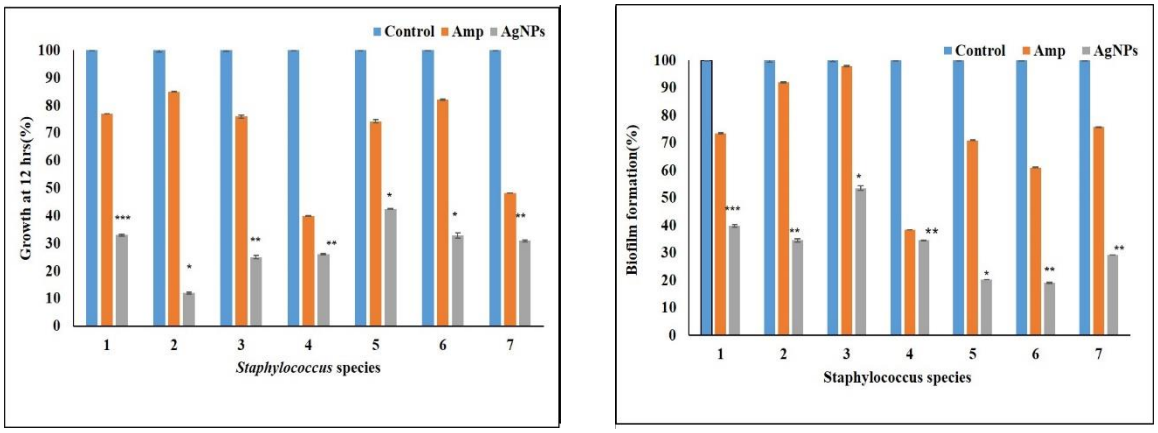


**(a)** **(b)**

**Figure 3.** Effect of AgNPs on growth and biofilm formation in different *Staphylococcus* species. **(a)** Percentage of bacterial growth after 12 hours of treatment; **(b)** Percentage of biofilm formation after 48 hours of treatment with AgNPs, compared with untreated control and Ampicillin (Amp). Whereas 1-MTCC, 2-MRSA, 3-MDR *Staphylococcus aureus* human isolates, 4-*Staphylococcus arlettae*, 5-*Staphylococcus cohnii* poultry isolates, 6-*Staphylococcus sciuri*, 7-*Staphylococcus chromogenes* cow mastitis isolates, AuNP-treated groups showed statistically significant differences from the control group by Student's t-test ($p < 0.05$).

MBC was 50 µg/ml for MRSA, 100 µg/ml for MDR, and 50 µg/ml. The AgNPs tolerance level was 4 µg/ml for MRSA, 2 µg/ml for MTCC, and 1 µg/ml for MDR, which represent bacteriostatic properties. MBC of *S. arlettae* 100 %, *S. cohnii* 100 %, *S. sciuri* 100 %, *S. chromogenes* 100 %. The tolerance level of silver nanoparticles was 12 µg/ml for *S. arlettae*, 2 µg/ml for *S. cohnii*, 8 µg/ml for *S. sciuri*, and 4 µg/ml for *S. chromogenes*, which represents the bacteriostatic property of AgNPs (Table 2).

**Table 2.** MIC, MBC, and tolerance level of Staphylococcus sp treated with AgNPs.

| ***Staphylococcus* sp.** | **MBC AgNPs µg/ml** | **MIC AgNPs µg/ml** | **MBC/MIC** |
|---|---|---|---|
| MRSA | 50 | 12.5 | 4 |
| MTCC | 100 | 50 | 2 |
| MDR | 50 | 50 | 1 |

| *Staphylococcus* sp. | MBC AgNPs µg/ml | MIC AgNPs µg/ml | MBC/MIC |
|---|---|---|---|
| *S. arlettae* | 100 | 6.25 | 16 |
| *S. cohnii* | 100 | 50 | 2 |
| *S. sciuri* | 100 | 12.5 | 8 |
| *S. chromogenes* | 100 | 12.5 | 8 |

The MIC provides a quantitative measure of the antimicrobial efficacy of AgNPs. Lower MIC values indicate higher effectiveness, as less material is mandatory to prevent microbial growth. The MIC of AgNPs provides essential information on the MIC required to inhibit bacterial growth effectively. It is a critical parameter for optimizing the use of AgNPs in diverse applications where precise, efficient antimicrobial activity is needed. Factors affecting MIC of AgNPs include nanoparticle size and shape, surface modification, concentration and dispersion, bacterial strain and resistance, and the mechanisms that, at the MIC concentration, effectively inhibit bacterial growth without additional toxic effects that higher doses might cause [28].

Biofilm assay was performed in MIC plates after 48 hours of incubation. Biofilm formation is reduced in AgNPs treatment than in control [29-32]. The proportion of biofilm formation was lowered to 34.59% in MRSA, 39.89 % in MTCC, and 53.6 % in MDR (Figure 3b). Biofilm formation in *Staphylococcus arlettae was 34.61* %, *Staphylococcus cohnii* 20.3 %, *Staphylococcus sciuri* 19.14 %, and 29.29 % *in Staphylococcus chromogenes*, as shown in Figure 3b. AgNPs are effective in reducing biofilm formation more significantly than ampicillin and the untreated control, as shown in Table 3. This suggests that AgNPs not only inhibit planktonic (free-floating) bacterial growth at MIC levels but also exhibit a potent antibiofilm effect, a major advantage for treating persistent bacterial infections.

**Table 3.** MIC, MBC, and biofilm formation of green-synthesized AgNPs against different *Staphylococcus* species.

| Bacterial Strain | MIC (µg/mL) | MBC (µg/mL) | Biofilm formation (%) |
|---|---|---|---|
| *S. aureus* (MRSA) | 12.5 | 50 | 34.59 ± 0.8 |
| *S. aureus* (MTCC) | 50 | 100 | 39.89 ± 1.2 |
| *S. aureus* (MDR) | 50 | 50 | 53.60 ± 1.0 |
| *S. arlettae* | 6.25 | 100 | 34.61 ± 0.9 |
| *S. cohnii* | 50 | 100 | 20.30 ± 0.7 |
| *S. sciuri* | 12.5 | 100 | 19.14 ± 0.5 |
| *S. chromogenes* | 12.5 | 100 | 29.29 ± 0.6 |

Values represent the mean ± SD of triplicate experiments (n = 3). MIC – Minimum Inhibitory Concentration; MBC – Minimum Bactericidal Concentration.

AgNPs can penetrate biofilm layers and disrupt bacterial cells through multiple mechanisms, such as ROS production and interference with bacterial cell membranes, DNA, and proteins. These mechanisms can hinder biofilm development at various stages, from initial attachment to mature biofilm. AgNPs can significantly reduce biofilm formation and may serve as a potent alternative or complementary agent to traditional antibiotics like ampicillin. Their ability to inhibit biofilms at MIC levels is promising for applications against stubborn, biofilm-associated infections [33]. Since biofilms are more resistant than planktonic bacteria, treatments often require higher antibiotic concentrations, which can lead to toxicity and resistance. AgNPs' antibiofilm effect at MIC levels could allow lower dosages and minimize these risks.

*3.3. AgNPs Effect on the reduction of proteins and sugars in Staphylococcus sp.*

*Staphylococcus* sp. treated with AgNPs at their MIC concentration showed high leakage of protein, nanoparticles caused leakage of proteins which was estimated by Bardford's method, cells treated with AgNPs showed high level of protein release than in ampicillin treated cells as shown in Figure 4a, previous studies revealed high leakage of protein in nanoparticles treated cells were due to alteration in cell membrane, rupture of cell wall and damage caused to cell wall structure, components. Leakage of protein is higher in *Staphylococcus chromogenes* than in other *Staphylococcus* sp. [27, 34].

Sugar leakage was greater in cells treated with AgNPs. *Staphylococcus sciuri* and *Staphylococcus chromogenes* showed higher leakage of sugars. Previous studies reported that sugar leakage is due to AgNPs penetrating the cell membrane, as shown in Figure 4b. The results clearly reveal that AgNPs exert antibacterial activity by penetrating through the cell membrane and by increasing the release of sugar and protein.

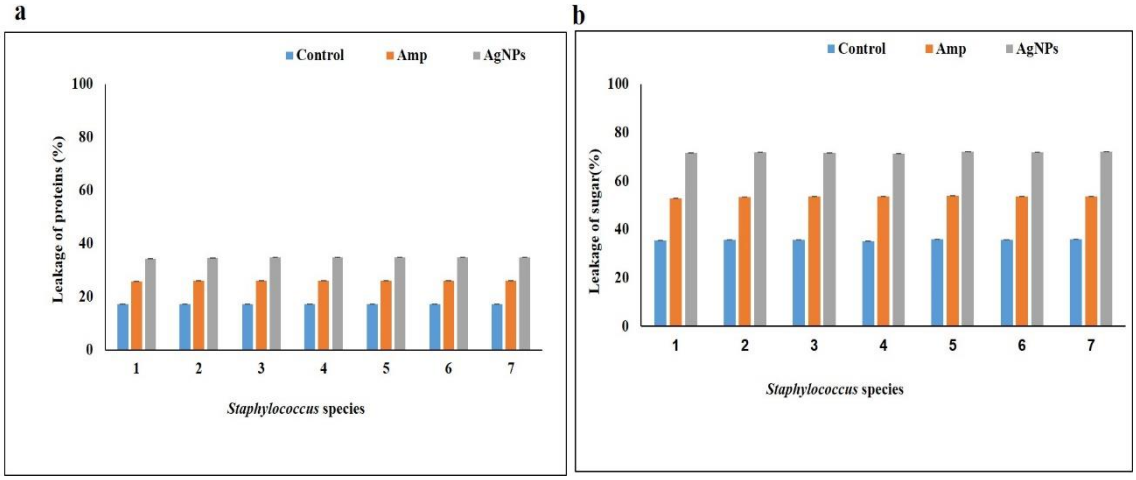


**Figure 4.** Leakage of biomolecules in *Staphylococcus* species treated with AgNPs. **(a)** Protein leakage; **(b)** sugar leakage observed in different *Staphylococcus* species upon treatment with AgNPs, indicating membrane disruption and cellular damage. Whereas 1-MTCC, 2-MRSA, 3-MDR *Staphylococcus aureus* human isolates, 4-*Staphylococcus arlettae*, 5-*Staphylococcus cohnii* poultry isolates, 6-*Staphylococcus sciuri*, 7-*Staphylococcus chromogenes* cow mastitis isolates.

*3.4. AgNPs' effect on antioxidant levels of Staphylococcus sp.*

Glutathione was used to measure the ROS production, and GSH levels were measured in *Staphylococcus* treated with AgNPs and ampicillin. There was a slight reduction in GSH levels in AgNPs-treated cells; this suggests that the elevated ROS observed in these cells was due to GSH depletion, leading to oxidative stress and loss of cell viability (Figure 5a). Previous studies also reveal that GSH depletion leads to oxidative stress and that AgNPs induce oxidative stress and disrupt cellular homeostasis [27, 34].

Oxidative stress was caused by an imbalance between pro-oxidants and antioxidants in cells. Environmental stress induces intracellular ROS and increases bacterial susceptibility, which also increases ROS production. The interaction between AgNPs and microbial cells results in the production of ROS, which induces oxidative stress and damages proteins and nucleic acids. Oxidative stress was measured in *Staphylococcus* sp., and malondialdehyde, a biomarker of oxidative stress, was measured in *Staphylococcus* sp. treated with AgNPs and ampicillin. Results showed that malondialdehyde was higher in AgNPs-treated cells than in ampicillin and control cells, as shown in Figure 5b. Previous studies also show that

malondialdehyde levels were higher in nanoparticle-treated cells, indicating increased oxidative stress. Several recent mechanistic studies and reviews report the same triad of effects for biosynthesized AgNPs and link these biochemical changes to reduced viability and disrupted biofilms. Thus, our oxidative stress and enzyme inhibition data are consistent with the dominant mechanistic model for plant-derived AgNPs. The statistical analysis of biochemical parameters is presented in Table 4.

**Table 4.** Simulated one-way ANOVA results for biochemical parameters.

| Parameter | F-value | p-value | Significance |
|---|---|---|---|
| **Protein leakage** | 0.36 | 0.889 | Not significant |
| **Sugar leakage** | 3.32 | 0.030 | Significant (p |
| **MDA** | 679.66 | $1.96 \times 10^{-16}$ | Highly significant |
| **GSH** | 45.69 | $2.11 \times 10^{-8}$ | Highly significant |
| **SOD** | 917.65 | $2.42 \times 10^{-17}$ | Highly significant |
| **Catalase** | 385.60 | $1.01 \times 10^{-14}$ | Highly significant |

Reactive oxygen species related enzymes SOD and catalase was evaluated in AgNPs treated and untreated *Staphylococcus* sp, results revealed that the nanoparticles treated cells had lower level of SOD (Figure 5c) and catalase (Figure 5d) than in control which implies modulation in antioxidant activity, this study and previous studies show that AgNPs is an oxidative shock inducer agents that cause cell death in Staphylococcus sp. A clear correlation was observed between oxidative stress induction and antibacterial activity. Treatment with AgNPs led to increased lipid peroxidation (elevated MDA levels) and depletion of antioxidant defenses (reduced GSH, SOD, and CAT activities), indicating ROS-mediated disruption of cellular components. This oxidative imbalance corresponded with reduced bacterial growth and biofilm integrity [34].

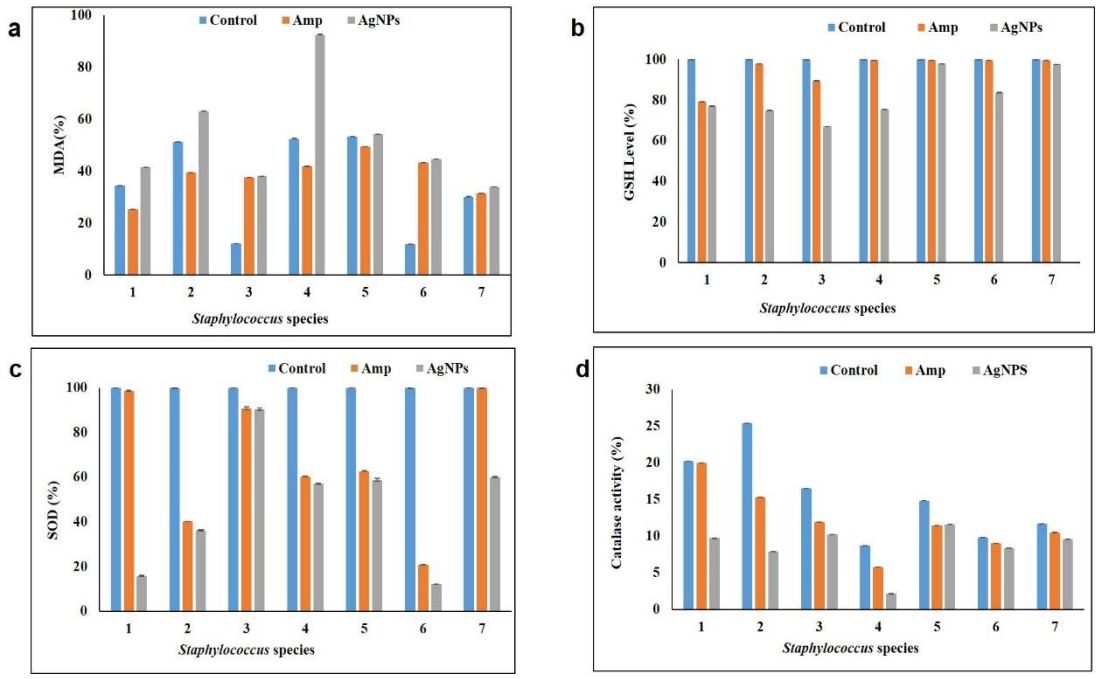


**Figure 5.** Oxidative stress and antioxidant enzyme activity in *Staphylococcus* species treated with AgNPs. **(a)** Malondialdehyde (MDA) levels indicating lipid peroxidation; **(b)** Reduced glutathione (GSH) content representing intracellular antioxidant status; **(c)** Superoxide dismutase (SOD) activity; **(d)** Catalase activity measured in untreated and AgNP-treated *Staphylococcus* cells, Whereas 1-MTCC, 2-MRSA, 3-MDR *Staphylococcus aureus* human isolates, 4-*Staphylococcus arlettae*, 5-*Staphylococcus cohnii* poultry isolates, 6-*Staphylococcus sciuri*, 7-*Staphylococcus chromogenes* cow mastitis isolates.

AgNPs induced ROS production, GSH depletion, and enzymes inactivation, SOD activity was highly reduced in MRSA and in *Staphylococcus sciuri*, nanoparticles regulate enzymatic activity, previous studies reveal that nanoparticles cause cell membrane disruption causing oxidative stress and also increase membrane permeability which leads to down regulation of antioxidant molecule GSH and also cause denaturation of enzymes that impairs the ETC pathway and leads to cell death [35, 36].

AgNPs showed high efficacy, and it reduced the growth of resistant *Staphylococcus* sp., AgNPs destroy the cell membrane permeability by destroying the cell membrane by generating many gaps and pits in the cell membrane.

## 4. Conclusions

This study demonstrated the green synthesis of silver nanoparticles using *Alpinia officinarum* rhizome extracts, as confirmed by comprehensive physicochemical characterization. The biosynthesized AgNPs exhibited potent antibacterial and antibiofilm activities against *Staphylococcus* species from human, poultry, and bovine sources, emphasizing their potential as eco-friendly antimicrobial agents.

Beyond confirming their efficacy, the results suggest that the phytochemicals of A. officinarum play a crucial role in nanoparticle stabilization and enhanced antibacterial performance by inducing oxidative stress and disrupting antioxidant enzyme balance. However, the study is limited by high particle polydispersity, the absence of in vivo validation, and a lack of data on Gram-negative pathogens, which may restrict broader applicability.

Future research should focus on toxicity evaluation, long-term stability assessment, in vivo efficacy testing, and comparative studies against Gram-negative and biofilm-forming bacteria. Moreover, integrating AgNPs with existing antimicrobial or wound-healing agents could provide synergistic therapeutic benefits and improve translational potential.

## Author Contributions

Conceptualization, H.S.; methodology, H.S., and N.A.; validation, H.S., and N.A.; formal analysis, N.A.; investigation, H.S.; data curation, N.A.; writing—original draft preparation, N.A.; writing—review and editing, H.S.; visualization, N.A.; supervision, H.S.; project administration, H.S.;. All authors have read and agreed to the published version of the manuscript.

## Institutional Review Board Statement

Not applicable.

## Informed Consent Statement

Not applicable.

## Data Availability Statement

Data supporting the findings of this study are available upon reasonable request from the corresponding author.

## Funding

This research received no external funding.

## Acknowledgments

The authors are thankful to B.S Abdur Rahman Institute of Science and Technology, Chennai, for providing research facilities in the School of Life Sciences.

## Conflicts of Interest

The authors declare no conflict of interest.

## References

1. Ma, X.; Tian, Y.; Yang, R.; Wang, H.; Allahou, L.W.; Chang, J.; Williams, G.; Knowles, J.C.; Poma, A. Nanotechnology in healthcare, and its safety and environmental risks. *J. Nanobiotechnol.* **2024**, *22*, 715, https://doi.org/10.1186/s12951-024-02901-x.
2. Mohamed Yunus Saleem, N.F.; Soundhararajan, R.; Srinivasan, H. Antimicrobial potential of floral extract-decorated nanoparticles against food-borne pathogens. *Discover Nano* **2025**, *20*, 103, https://doi.org/10.1186/s11671-025-04292-w.
3. Keskin, C.; Aslan, S.; Baran, M.F.; Baran, A.; Eftekhari, A.; Adıcan, M.T.; Ahmadian, E.; Arslan, S.; Mohamed, A.J. Green Synthesis and Characterization of Silver Nanoparticles Using *Anchusa Officinalis*: Antimicrobial and Cytotoxic Potential. *Int. J. Nanomed.* **2025**, *20*, 4481-4502, https://doi.org/10.2147/IJN.S511217.
4. Trivedi, S.; Srivastava, A.; Saxena, D.; Ali, D.; Alarifi, S.; Solanki, V.S.; Agarwal, N.; Kumar, S.; Banerjee, M.; Niazi, P.; Yadav, V.K. Phytofabrication of silver nanoparticles by using *Cucurbita maxima* leaf extract and its potential anticancer activity and pesticide degradation. *Mater. Technol.* **2025**, *40*, 2440907, https://doi.org/10.1080/10667857.2024.2440907.
5. Gunasekaran, V.V.; Ranjani, S.; Hemalatha, S. Sustainable and eco-friendly silver nanoparticles synthesized from *Arachis hypogaea* nutshell extract to control phytopathogens. *Environ. Sci. Eur.* **2025**, *37*, 142, https://doi.org/10.1186/s12302-025-01171-0.
6. Al-Sahlany, S.T.; Niamah, A.K.; Verma, D.K.; Prabhakar, P.; Patel, A.R.; Thakur, M.; Singh, S. Applications of Green Synthesis of Nanoparticles Using Microorganisms in Food and Dairy Products: Review. *Processes* **2025**, *13*, 1560, https://doi.org/10.3390/pr13051560.
7. Juzer, T.; Soundharajan, R.; Srinivasan, H. *Camellia sinensis* mediated silver nanoparticles: eco-friendly antimicrobial agent to control multidrug resistant Gram-positive *Staphylococcus aureus*. *Discover Nano* **2025**, *20*, 92, https://doi.org/10.1186/s11671-025-04278-8.
8. Ito, Y.; Sasaki, T.; Li, Y.; Tanoue, T.; Sugiura, Y.; Skelly, A.N.; Suda, W.; Kawashima, Y.; Okahashi, N.; Watanabe, E.; Horikawa, H.; Shiohama, A.; Kurokawa, R.; Kawakami, E.; Iseki, H.; Kawasaki, H.; Iwakura, Y.; Shiota, A.; Yu, L.; Hisatsune, J.; Koseki, H.; Sugai, M.; Arita, M.; Ohara, O.; Matsui, T.; Suematsu, M.; Hattori, M.; Atarashi, K.; Amagai, M.; Honda, K. *Staphylococcus cohnii* is a potentially biotherapeutic skin commensal alleviating skin inflammation. *Cell Reports* **2021**, *35*, 109052, https://doi.org/10.1016/j.celrep.2021.109052.
9. De Mel, S.; Gruenler, J.; Khoury, L.; Heynes, A.; Fazekas, J.; Damaske, K.; Galbadage, T.; Gunasekera, R.S.; Anderson, R.S. Green synthesis of silver nanoparticles using *Magnolia alba* leaf extracts and evaluating their antimicrobial, anticancer, antioxidant, and photocatalytic properties. *Sci. Rep.* **2025**, *15*, 23709, https://doi.org/10.1038/s41598-025-08468-3.
10. Ghasemi, S.; Dabirian, S.; Kariminejad, F.; Koohi, D.E.; Nemattalab, M.; Majidimoghadam, S.; Zamani, E.; Yousefbeyk, F. Process optimization for green synthesis of silver nanoparticles using *Rubus discolor* leaves extract and its biological activities against multi-drug resistant bacteria and cancer cells. *Sci. Rep.* **2024**, *14*, 4130, https://doi.org/10.1038/s41598-024-54702-9.
11. Lienen, T.; Schnitt, A.; Hammerl, J.A.; Marino, S.F.; Maurischat, S.; Tenhagen, B.-A. Multidrug-resistant *Staphylococcus cohnii* and *Staphylococcus urealyticus* isolates from German dairy farms exhibit resistance

to beta-lactam antibiotics and divergent penicillin-binding proteins. *Sci. Rep.* **2021**, *11*, 6075, https://doi.org/10.1038/s41598-021-85461-6.

12. Parmanik, A.; Kothari, P.P.; Bose, A.; Biswas, S. Evaluation of antibacterial and antibiofilm activities of green-synthesized iron oxide nanoparticles using *Cyperus rotundus* extract as a reducing and stabilizing agent. *J. Mater. Sci.: Mater. Med.* **2025**, *36*, 60, https://doi.org/10.1007/s10856-025-06914-2.
13. Pasieczna-Patkowska, S.; Cichy, M.; Flieger, J. Application of Fourier Transform Infrared (FTIR) Spectroscopy in Characterization of Green Synthesized Nanoparticles. *Molecules* **2025**, *30*, 684, https://doi.org/10.3390/molecules30030684.
14. Kumar, D.; Soundhararajan, R.; Srinivasan, H. *Green synthesis and characterization of Triphala $SiO_2$ nanoparticles and screening the efficacy on growth and biochemical constituents in Vigna radiata*. *Discover Nano* **2025**, *20*, 88, ttps://doi.org/10.1186/s11671-025-04268-w
15. Soundhararajan, R.; Srinivasan, H. Multidrug-resistant Bacillus species isolated from hospital soil environment is controlled by nanobiotics incorporated nanoformulation. *Environmental Research* **2024**, *246*, 118122, https://doi.org/10.1016/j.envres.2024.118122.
16. Suha Kouser I.; Soundhararajan, R.; Srinivasan, H. *Camellia sinensis-mediated nanoparticles to control growth and biofilm in* Vibrio sp. *Aquaculture International* **2025**, *33*(3), 204, https://doi.org/10.1007/s10499-025-01887-z.
17. Basha, S. B. A.; Soundhararajan, R.; Srinivasan, H. Solanum virginianum-mediated green nanoparticles to control dental pathogens. *Discover Applied Sciences* **2025**, *7*, **67**, https://doi.org/10.1007/s42452-025-06469-5
18. Talib, H.; Mehmood, A.; Amjad, M.S.; Mustafa, A.; Khan, M.A.R.; Raffi, M.; Khan, R.T.; Ahmad, K.S.; Qureshi, H. Antibacterial, antioxidant, and anticancer potential of green fabricated silver nanoparticles made from *Viburnum grandiflorum* leaf extract. *Bot. Stud.* **2024**, *65*, 4, https://doi.org/10.1186/s40529-024-00411-5.
19. Jiang, X.; Khan, S.; Dykes, A.; Stulz, E.; Zhang, X. Biogenic Synthesis of Silver Nanoparticles and Their Diverse Biomedical Applications. *Molecules* **2025**, *30*, 3104, https://doi.org/10.3390/molecules30153104.
20. Singh, H.; Desimone, M.F.; Pandya, S.; Jasani, S.; George, N.; Adnan, M.; Aldarhami, A.; Bazaid, A.S.; Alderhami, S.A. Revisiting the green synthesis of nanoparticles: uncovering influences of plant extracts as reducing agents for enhanced synthesis efficiency and its biomedical applications. *Int. J. Nanomed.* **2023**, *18*, 4727-4750, https://doi.org/10.2147/IJN.S419369.
21. Altammar K.A. A review on nanoparticles: characteristics, synthesis, applications, and challenges. *Front. Microbiol.* **2023**, *14*, 1155622, https://doi.org/10.3389/fmicb.2023.1155622.
22. Eker, F.; Akdaşçi, E.; Duman, H.; Bechelany, M.; Karav, S. Green Synthesis of Silver Nanoparticles Using Plant Extracts: A Comprehensive Review of Physicochemical Properties and Multifunctional Applications. *Int. J. Mol. Sci.* **2025**, *26*, 6222, https://doi.org/10.3390/ijms26136222.
23. Todorova, M.; Petrova, V.; Ranguelov, B.; Avdeev, G.; Velkova, L.; Atanasova-Vladimirova, S.; Pisareva, E.; Tankov, C.; Tomova, A.; Dolashki, A.; Dolashka, P. Green Synthesis of Antimicrobial Silver Nanoparticles (AgNPs) from the Mucus of the Garden Snail *Cornu aspersum*. *Molecules* **2025**, *30*, 2150, https://doi.org/10.3390/molecules30102150.
24. Asefian, S.; Ghavam, M. Green and environmentally friendly synthesis of silver nanoparticles with antibacterial properties from some medicinal plants. *BMC Biotechnol.* **2024**, *24*, 5, https://doi.org/10.1186/s12896-023-00828-z.
25. Ranjani, S.; Priya, P.S.; Veerasami, M.; Hemalatha, S. Novel Polyherbal Nanocolloids to Control Bovine Mastitis. *Appl. Biochem. Biotechnol.* **2022**, *194*, 246-265, https://doi.org/10.1007/s12010-021-03748-w.
26. Swolana, D.; Wojtyczka, R.D. Activity of Silver Nanoparticles against *Staphylococcus* spp. *Int. J. Mol. Sci.* **2022**, *23*, 4298, https://doi.org/10.3390/ijms23084298.
27. NajeerAhamed, M.J.; Soundharajan, R.; Srinivasan, H. Antibacterial, antibiofilm, and antivirulence effects of nanoparticles synthesized from *Colletotrichum gloeosporioides* in pathogenic *E. coli*. *Microb. Pathog.* **2023**, *185*, 106420, https://doi.org/10.1016/j.micpath.2023.106420.
28. Rani, N.; Rani, S.; Patel, H.; Bhavna; Yadav, S.; Saini, M.; Rawat, S.; Saini, K. Characterization and investigation of antioxidant and antimicrobial activity of zinc oxide nanoparticles prepared using leaves extract of *Nyctanthes arbor-tristis*. *Inorg. Chem. Commun.* **2023**, *150*, 110516, https://doi.org/10.1016/j.inoche.2023.110516.

29. Mulu, M.; Tefera, M.; Guadie, A.; Basavaiah, K. Biosynthesis, characterization and study of the application of silver nanoparticle for 4-nitrophenol reduction, and antimicrobial activities. *Biotechnol. Rep.* **2024**, *42*, e00838, https://doi.org/10.1016/j.btre.2024.e00838.
30. Iravani, S.; Varma, R. S. Green synthesis, biomedical, and biological applications of silver nanoparticles: recent advances and future prospects. *Journal of Nanostructure in Chemistry* **2023**, *13*, 43. https://doi.org/10.1007/s40097-022-00493-5.
31. Fares, A.; Mahdy, A.; Ahmed, G. Unraveling the mysteries of silver nanoparticles: synthesis, characterization, antimicrobial effects and uptake translocation in plant—a review. *Planta* **2024**, 260, 7, https://doi.org/10.1007/s00425-024-04439-6.
32. Fahim, M.; Shahzaib, A.; Nishat, N.; Jahan, A.; Bhat, T.A.; Inam, A. Green synthesis of silver nanoparticles: A comprehensive review of methods, influencing factors, and applications. *JCIS Open* **2024**, *16*, 100125, https://doi.org/10.1016/j.jciso.2024.100125.
33. Dar, N.A.; Dar, P.A.; Qadir, M.; Shah, W.A. Green synthesis and characterization of bioactive silver nanoparticles from *Stachys tibetica*. *Sci. Rep.* **2025**, *15*, 29673, https://doi.org/10.1038/s41598-025-92507.
34. Shahzadi, S.; Fatima, S.; ul ain, Q.; Shafiq, Z.; Janjua, M.R.S.A. A review on green synthesis of silver nanoparticles (SNPs) using plant extracts: a multifaceted approach in photocatalysis, environmental remediation, and biomedicine. *RSC Adv.* **2025**, *15*, 3858-3903, https://doi.org/10.1039/D4RA07519F.
35. Saba, M.; Farooq, S.; Alessa, A.H.; Bektas, K.I.; Belduz, A.O.; Khan, A.Z.; Shah, A.A.; Badshah, M.; Khan, S. Green synthesis of silver nanoparticles using Keratinase from *Pseudomonas aeruginosa*-C1M, characterization and applications as novel multifunctional biocatalyst. *BMC Biotechnol.* **2025**, *25*, 27, https://doi.org/10.1186/s12896-025-00959-5.
36. Ibrahim, N.A.A.; Saeed, H.A.; Saeed, S.M.; Mohamed, O.; Suliman, O.H.; Ibrahim, S.A.E.; Mohamed, S.B. Green synthesis of silver nanoparticles using Sudanese *Candida parapsilosis*: a sustainable approach to combat antimicrobial resistance. *BMC Microbiol.* **2025**, *25*, 312, https://doi.org/10.1186/s12866-025-04038-9.

## Publisher's Note & Disclaimer